Reversibility of granular rotations and translations

Anton Peshkov, Michelle Girvan, Derek C. Richardson, and Wolfgang Losert

Phys. Rev. E **100**, 042905 — Published 11 October 2019

DOI: 10.1103/PhysRevE.100.042905

On the reversibility of granular rotations and translations

Anton Peshkov,[1] Michelle Girvan,[2] Derek C. Richardson,[3] and Wolfgang Losert[2]
[1] *IREAP, University of Maryland, College Park, Maryland, USA*
[2] *Departments of Physics, IPST and IREAP, University of Maryland, College Park, Maryland, USA*
[3] *Department of Astronomy, University of Maryland, College Park, Maryland, USA*

We analyze reversibility of displacements and rotations of spherical grains in three-dimensional compression experiments. Using transparent acrylic beads with cylindrical holes and index matching techniques, we are not only capable of tracking displacements but also, for the first time, analyzing reversibility of rotations. We observe that for moderate compression amplitudes, up to one bead diameter, the translational displacements of the beads after each cycle become mostly reversible after an initial transient. By contrast, granular rotations are largely irreversible. We find a weak correlation between translational and rotational displacements, indicating that rotational reversibility depends on more subtle changes in contact distributions and contact forces between grains compared with displacement reversibility. 3D rotations in dense granular systems are particularly important, since frictional losses associated with rotations are the dominant mechanism for energy dissipation. As such our work provides a first step toward a thorough study of rotations and tangential forces to understand the granular dynamics in dense systems.

I. INTRODUCTION

Flows of granular matter are an important subject of study in many fields, including geology (where they are relevant for avalanches and earthquakes), engineering (where they play a role in industrial processes and construction), and astronomy (where they affect the formation of asteroids and planets). In these contexts, it is particularly important to understand how the granular material transitions from a jammed state to a state of flow with irreversible rearrangements. A common driver of granular flow are cyclic perturbations, which can be caused by a wide range of driving forces, such as vibrating apparatus (construction), periodic loads (roads and rails), earthquakes, cyclic gravitational fields (tidal forces), or thermal expansion and contraction due to day/night temperature variations (on planets and asteroids). Beside the question of flows, the cycling compression or shearing of the granular system can change the properties of the packing, leading to compaction [1] and ultimately crystallization in some cases [2, 3].

Most past numerical and experimental work in this area has concentrated on the translational motion of particles and the associated force fields. However, granular systems are frictional and often aspherical, which implies the presence of rotations of the grains. Rotations and torques can play an important role in mesoscopic granular motions, as has been shown in two-dimensional investigations [4]. Thus bulk granular mechanics is affected by both force networks and torques, though rotations and torques are often ignored, with the notable exception of the Cosserat continuum elastic models [5].

Furthermore, rotations are likely more important in a frictional three dimensional system, where friction will increase the number of constraints from 3 to 6. Compare this to a model two dimensional system with an increase from 2 to 3. Frictional, rotating, systems can become isostatic with four contacts per particle, long before the jamming point at 6 contacts per particle [1] and are therefore over-constrained. The distribution of frictional forces is dependent on the history of contacts [6], i.e., the method of preparation of the system. Periodic compression will alter the contact distribution and could lead to a different state of the system, called a random loose packing, in contrast to the random close packing with six contacts per particle that we would find for a frictionless system. Thus understanding rotations is important to elucidate the nature of different jammed states of frictional spherical (or aspherical) particles as well as their transition to flow.

Despite the importance of rotations for granular systems, only a handful of experimental investigations have studied them [7, 8], especially in three dimensions [9–13]. In this study of reversibility we build on our first experimental measurements of particle-scale rotations in a three-dimensional granular flow [14], and systematically measure both rotations and translations under cyclic forcing. To focus our investigation on irreversibilities associated with rotational motion, we study small enough driving amplitudes so that the translational motion of the system is reversible. We had previously shown that in this small forcing regime, convective flows and segregation—two hallmarks of bulk granular flow—are also suppressed [15].

II. EXPERIMENTAL SETUP

The experimental setup, sketched in figure 1(a), is composed of a container with transparent walls filled with transparent acrylic beads. The container is 15.24 cm wide (y direction) and approximately 15 cm long (x direction). The back wall is displaced by a motor to compress the whole system. The amplitude of compression was varied

between 0.5 % and 2.5 % of the container length. Note that we can not go beyond 3% with our setup, as it corresponds to the diameter of a single bead. Beyond this limit, the beads will jam between the weight placed on the beads and the moving wall. At these amplitudes, our experimental system is still below the convection regime, which will invariably appear at higher amplitudes [16]. The compression speed was 0.05 mm s^{-1} for all amplitudes, i.e. a constant shear rate. We verified that this speed is slow enough to expect granular rearrangements that resemble dry systems [17]. All the experiments contained between 500 and 1000 cycles of compression, with between 4 and 16 three-dimensional images captured during each cycle. All figures in the manuscript are presented for the case of 2.5 % compression, unless noted otherwise.

The container is filled with 20,000 transparent acrylic beads of radius $R = 2.5\,mm$, forming a height (z direction) of approximately twenty layers. Each bead has a $1.4\,mm$ diameter cylindrical cavity running through it, allowing us to detect the orientation of the bead. A $1.5\,kg$ transparent acrylic weight is placed on the beads to maintain a constant pressure. The beads and the weight are submerged in an index-matched solution of Triton X-100, which additionally includes a fluorescent Nile blue dye as well as 0.05 % of hydrochloric acid (38 % concentration) . The whole system is illuminated with two 660 nm, which approximately corresponds to the maximum excitation fluorescence frequency of Nile blue, scanning sheet lasers from both sides of the container.

We should note that a single hole in the grains does not allow us to detect rotations when the axis of rotations is along the hole of the bead. Only rotation components perpendicular to the hole can be resolved. Thus, our current experimental setup captures only a part of the rotation amplitude. However, in this work we focus on the statistical analysis of amplitudes of rotations, not taking into account such information as the axis of rotation or its correlation with other quantities. Given the small compression amplitude, the beads rotate less than $\pi/2$ between scans, preventing any degeneracy in the detection of rotations.

Typically four full scans of the system are performed per compression cycle, as shown in figure 1.b) : a scan before compression (time A), a scan at half-compression (B), a scan at full compression (C), a scan at half-decompression (D) and a scan at full decompression (E). The first and last 10 cycles are recorded with 16 scans per cycle. Most of the presented results are an average over the last 10 cycles of the experiment.

Positions and rotations are then extracted and tracked [14]. To directly compare the rotations and translations in the same units, we multiply all rotation angles by the radius of the bead. In the case of non-slip rolling of a bead on a flat surface, this will make the values of rotational and translation displacements identical. We have estimated the standard error on particle position detection to be $20\,\mu m$ and the standard error on angle detection to be $0.0345\,rad$ ($\sim 2°$) or $86\,\mu m$.

Crystallization occurs near the borders of the experimental cell, for the statistical analysis we omit all particles in this layers as well as in the bottom four layers, where optical aberrations lead to larger detection errors and all the particles whose motion during the compression cycle is less than the standard error.

III. VALIDATION OF THE EXPERIMENTAL APPROACH

The hole in the middle of the bead produce two "cavities" on the bead surface in which other beads can "fall". It is thus necessary to verify if the beads have a preference to form a contact at the cavities and if yes, to verify that it does not significatively change the results that we obtain.

Let us call α the angular oppening of the hole as shown on figure 2 a). A straitforward calculation will give

$$\alpha = 2\sin^{-1}\left(\frac{d}{D}\right)$$

where $D = 5\,mm$ is the diameter of the bead and $d = 1.4\,mm$ is the diameter of the hole. Given an axis passing through the hole, the cumulative probability that a contact point will be located within an angle $\beta \in [0 : \pi/2]$ of this axis is given by the surface area located within this angle. We can then easily show that this probability to be located within an angle β from any of the two holes is

$$\begin{aligned} P(\beta) &= 1 - \cos(\beta) \\ &= 1 - \sqrt{1 - \sin^2(\beta)} \end{aligned}$$

.

If we define a contact through a hole as any contact whose contact point is located within an angle $\alpha/2$ of the hole axis, then the theoretical probability of contacting through the hole is given by

$$\begin{aligned} P\left(\frac{\alpha}{2}\right) &= 1 - \sqrt{1 - \left(\frac{d}{D}\right)^2} \\ &= 4\,\% \end{aligned}$$

. To check this prediction we compute the probability of a contact hapening at a particular angle from the axis from our experimental data. To detect a contact we consider all beads located within a cuttof distance r_c as being in contact. The value of r_c is determinde as described in the part V of the article. We compute this probability both at the begining and the end of the experiment. The result is presented on figure 2 b). We can see that the actual probability of contacting through a hole is higher than the theoretically predicted value indicating that indeed

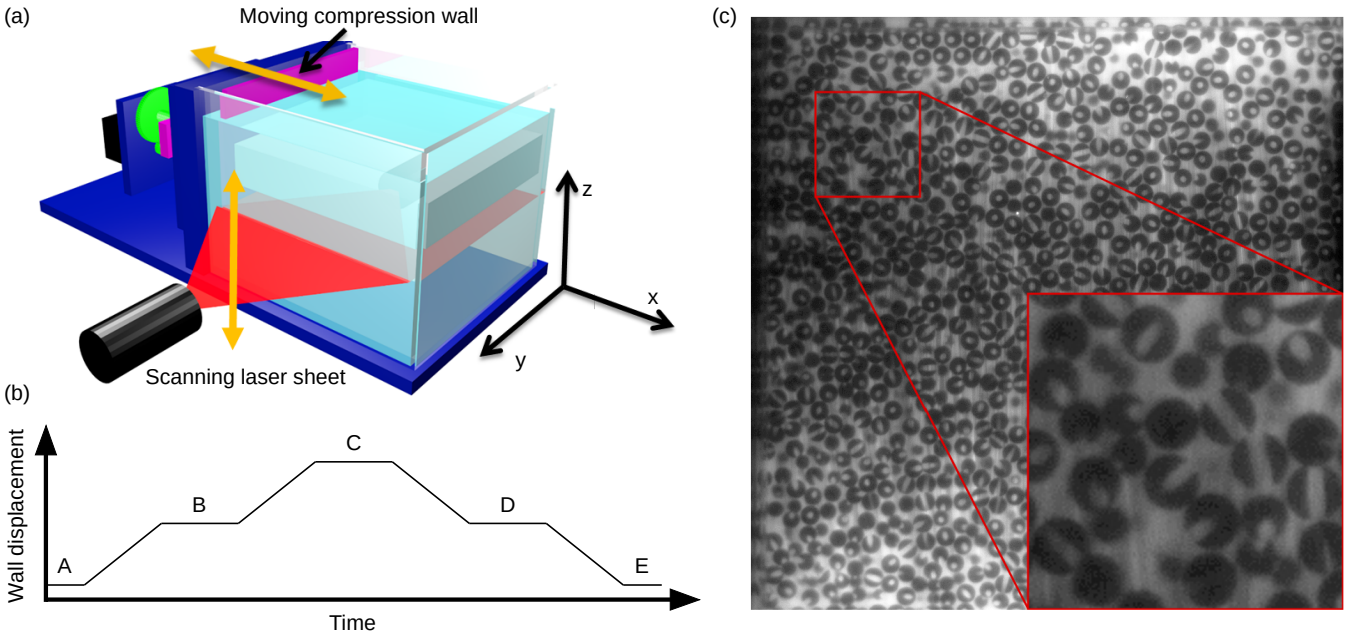

Figure 1. (a) Schematics of the setup. (b) Schematics of the 5 positions of the wall at which 3D scans are performed. Note that position E of the current cycle correspond to position A of the next cycle. (c) One example image of one hole beads - typically a sequence of 500 images is captured in each 3D scan. A whole scanning sequence can be seen in supplemental movies.

the particles tend to "fall" inside the hole. The experimental cummulative probability of contacting through the hole is $\approx 12\,\%$. Note that the increased probabily of a contact hapening through the hole, also increase the probability of a contact happening at 60° from the hole as explained on figure 2 a). This results are in good agreement with the predictions made for "shpero-cylindrical" particles [18]. However we can see that the probability of contacting through a hole is unchanged at the begining of the experiment as well as at the end of the experiment. This means that there is no any tendency for the "crystalization" of hole contacts.

We can ask the question if the particle contacting through a hole will see their dynamics impacted as to the particles which do not contact through the hole. For this end we measure the probability of translational and rotational displacements at times C and E as compared to the begining of the cycle. We measure these quantities separately for particles that do contact through a hole at the begining of the cycle and particles that do not. The results are presented on figure 3. We can see that the translations are unaffected by the type of contact. Only rotations suffer a small decrease in their amplitude while mantaining the overall shape of the distribution. Note that this decrease in rotational mobility emphasis even more our funding on the ireversibility of the rotational dynamics.

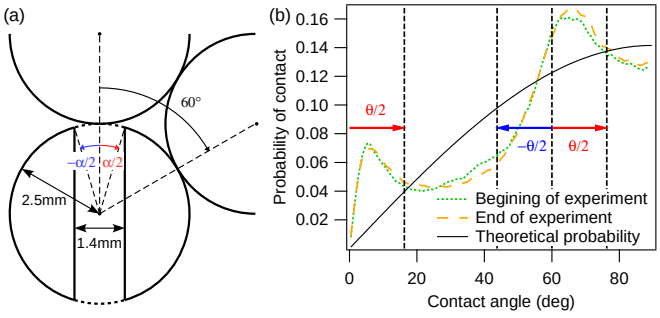

Figure 2. a) Sketch of the contact through a hole. Note that an increase in the probability of contacting through a hole will also increas the probability of a contact hapening at 60° from the hole axis. b) Experimental probability of a contact point being at a certain angle to the hole axis. Green dots indicate the begining of the experiment, yellow dash the end of experiment and black line the theoretical predicted value for an equal probability contact point. Results for 2.5% compression amplitude.

IV. TRANSLATIONAL AND ROTATIONAL DISPLACEMENTS

We denote by $\vec{x}_i^T$ the position of particle i at the temporal position T (one of A–E) in the cycle and by $\hat{q}_i^T$ its orientation expressed as a unit vector. We introduce the relative (as compared to the beginning of the cycle) displacements of particles at time T: the translational $\mu_i^T = \left\|\vec{x}_i^T - \vec{x}_i^A\right\|$ and the rotational $\theta_i^T = \sin^{-1}\left(\left\|\hat{q}_i^T \times \hat{q}_i^A\right\|\right)$, as well as their averages: $\left\langle \mu^T \right\rangle = \frac{1}{N}\sum_{i=1}^{N} \mu_i^T$ and $\left\langle \theta^T \right\rangle =$

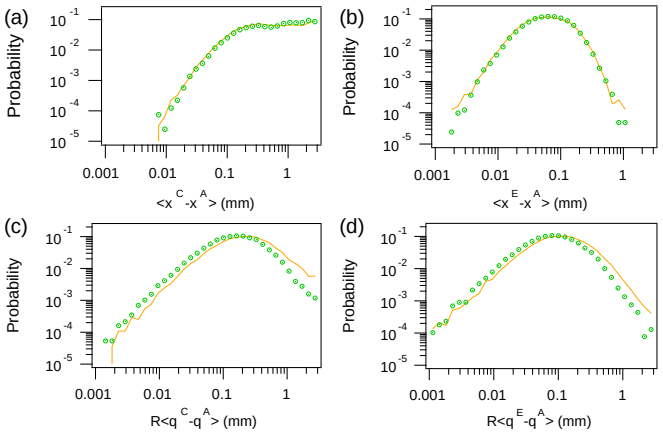

Figure 3. Probability of translational (a and b) and rotational (c and d) displacements between the begining and middle (a and c) and end (b and d) of cycle. Yellow line indicate particles that do not contact through their hole at the begining of the cycle, while green circles indicate particles that do contact through the hole. Displacement units in mm. Results for 2.5% compression amplitude.

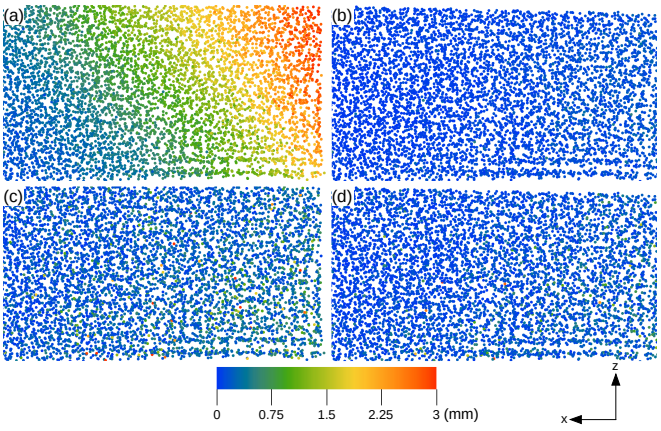

Figure 4. Two dimensional projections on the x-z plane of bead translational (a and b) and rotational (c and d) displacements between the begining and middle (a and c) and between the begining and end (b and d) of a cycle. The color indicate the amplitude of displacement. The compression wall is located to the right of the snapshots. All units in mm.

$\frac{1}{N}\sum_{i=1}^{N}\theta_i^T$.

Figure 4 a) shows a snapshot of typical translational displacements of the particles at time C. The gradient angle matches the symmetry of the system, with a compressing right wall and movable top wall kept at constant pressure. In contrast, the rotations, represented on the 4 c), do not present any apparent shear zones, with a larger concentration of rotations near the bottom of the cell, suggesting an absence of direct correlation between translations and rotations. This is corroborated by statistical analysis as presented below. Figure 4 b) and d) shows snapshots at the end of the cycle, at time E, of translations and rotations respectively. While most of the translational displacement of the particles is reversed, this is not the case for all rotations as discussed further.

Note that due to the nature of our experiments, a small but measurable compaction (following a power law) is found as expected [19] in our system. While the particle positions are not perfectly reversible, we focus on small amplitudes where particles retain their neighbors, and where (as shown in [15]) convection and segregation are suppressed. In this regime, where the position of most particles with respect to their neighbors is reversible, we investigate rotations, as well as their evolution with cycle number.

To examine the irreversibility of the granular motion we can study the translational and rotational displacements of particles at the end of the cycle: μ_i^E and θ_i^E. As can be seen in scatter plots of translations and rotations (figure 5), comparing the displacements of each particle at time C to the displacements at time E, translations are reversible as expected, while rotations are mostly irreversible with a lot of particles not returning to their initial orientation.

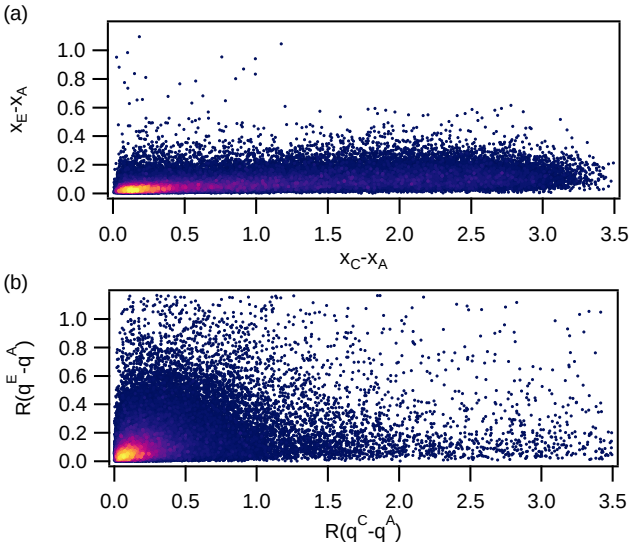

Figure 5. (a) Scatter plot of translations between the middle of the cycle and the end of cycle. (b) Same for rotations. The color indicates the beads density at the particular location. All units in mm. Results for 2.5% compression amplitude.

To obtain a better statistical understanding of the phenomena, we compare the expected end-of-cycle displacements μ^E and θ^E for given values of mid-cycle displacements μ^C and θ^C (figure 6). These are well characterized by power-law behaviors with approximate exponents of ≈ 0.35 for translations and ≈ 0.43 for rotations at moderate displacements. As seen in the figure, these exponents do not depend on the amplitude of compression of our system, indicating a universal behavior for the amplitudes we investigated. Note that such a behaviour could indicate an existence of strong temporal correlations for

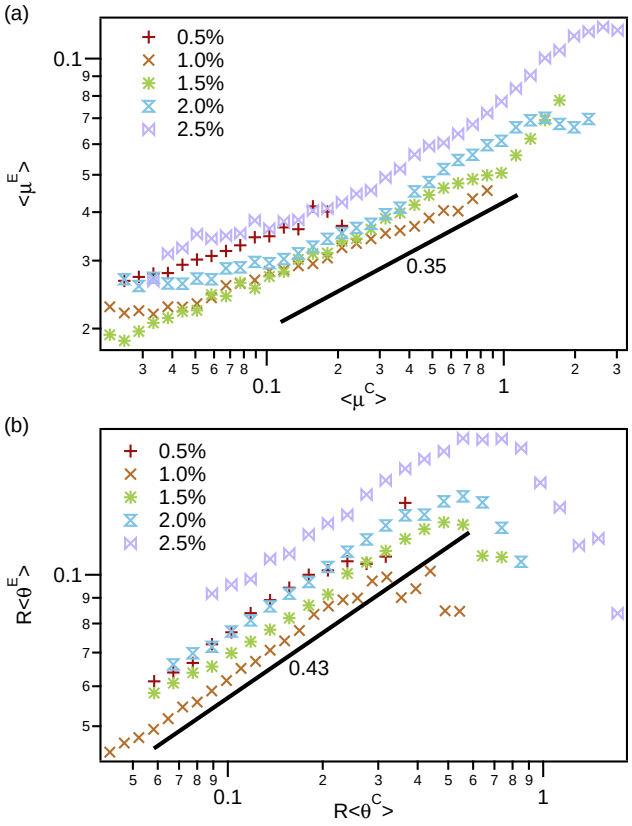

Figure 6. The expected end of cycle translational (a) and rotational (b) displacements as compared with the mid-cycle displacements, for different compression amplitudes. The solid lines illustrate power laws with exponents of 0.35 and 0.43. All units in mm.

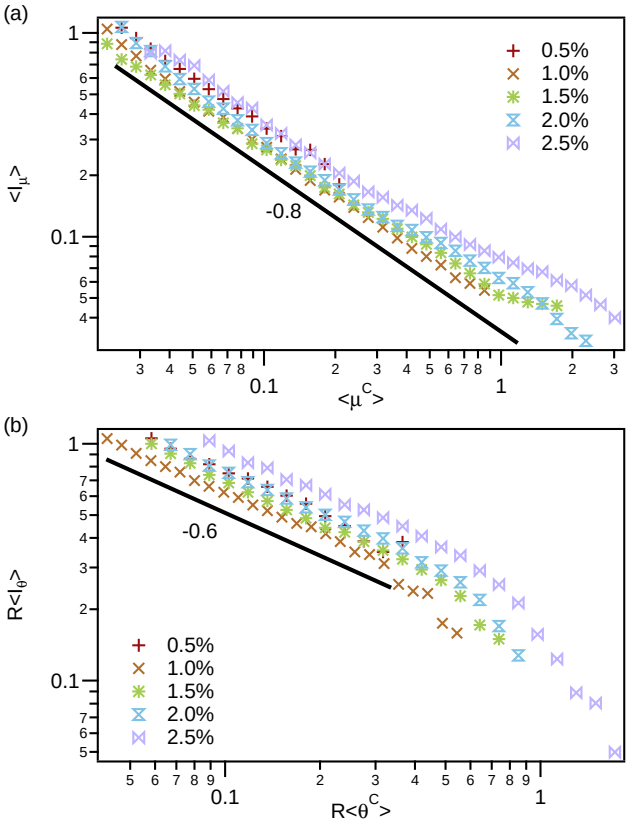

Figure 7. Relative irreversibility parameters I_μ (a) and I_θ(b) as a function of the mid-cycle mobility μ^C and θ^C for different compression amplitudes. All units in mm.

the translations and rotations[20].

At very large values of translation displacement the exponent seems to increase, probably corresponding to a transition to diffusive behavior when beads move so much that they can escape their "cage". Both the translational and rotational exponents are smaller than 1, which implies that the relative reversibility improves for bigger displacements. We introduce relative irreversibility parameters $I_{\mu,i} = \mu_i^E/\mu_i^C$ for translations and $I_{\theta,i} = \theta_i^E/\theta_i^C$ for rotations, which plotted against the mid-cycle displacements μ^C and θ^C give the expected mid-cycle exponents of ≈ -0.8 and ≈ -0.6 as seen on figure 7.

We have found that the expected middle or end-of-cycle rotational displacements $\theta^{C,E}$ and translational displacements $\mu^{C,E}$ are very weakly correlated, as can be seen on figure 8. This result is in contrast to the case of ellipsoidal particles, where a strong correlation between rotations and translations was experimentally found [12]. The difference can be explained by the fact that for ellipsoidal particles, rotations imply a change in the effective volume occupied by the particles and thus can couple to translations of surrounding particles.

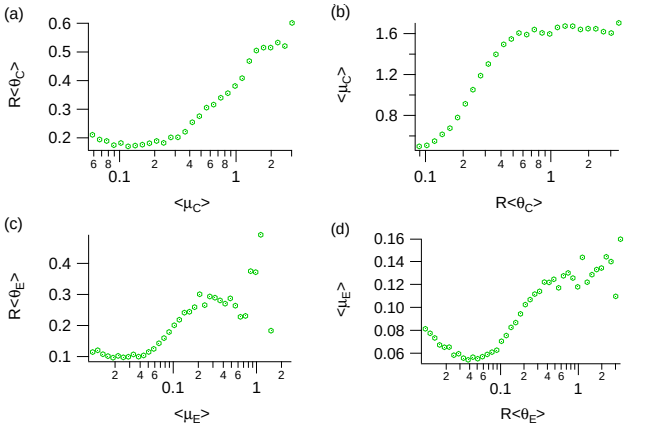

Figure 8. (a) Averaged value of rotational displacement binned over values of translational displacement at time C. (b) Averaged value of translational displacement binned over values of rotational displacement at state C. (c) and (d) same as (a) and (b) at time E. All units in mm.

Beyond the reversibility to its initial position and orientation, we investigate the reversibility of the whole particle trajectory, both in terms of translation and rotation. We plot the displacements of particles during a cycle of compression averaged over similar values of mid-cycle displacements (Fig. 9). These results are based on the actual motion of the moving wall, corrected for slight backlash present in our experimental system.

Figure 9 highlights the difference between the behavior of granular translations and rotations. Translations are very reversible, with beads following much of the same path during compression and dilation, especially at high values of the wall displacement. On the other hand, the rotation trajectories are much less so; the dilation path, which begins at maximum wall displacement and goes back to zero wall displacement, diverges almost immediately from the compression path. In other words, in contrast to the translations, the forward and backward paths for rotations differ significantly even close to point of wall reversal (maximum wall displacement). The reversibility of both translations and rotations improves after many cycles as compared with the beginning of the experiment (not shown), suggesting that, after an initial transient period, the system self-organizes into a more reversible configuration.

V. CONTACT DYNAMICS

For particles to revert back to their original positions relative to their neighbors without reversal of orientations requires some change in frictional contacts. To study the contacts dynamics, we define particles that are within a cutoff distance r_c of each other as being likely in contact. To capture all likely contacts we chose r_c as the distance within which particles have on average 6 contacts

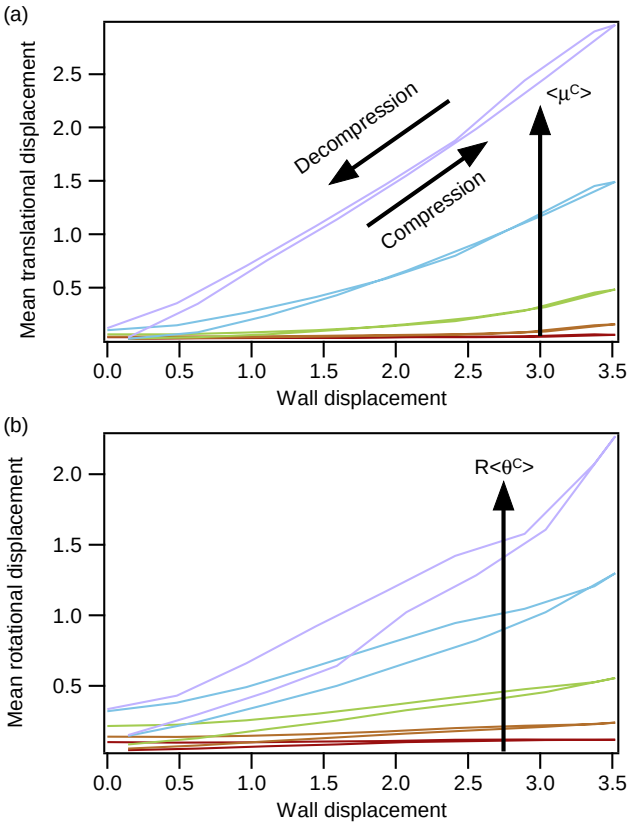

Figure 9. Mean translational displacement $\langle \mu^T \rangle$ trajectories (a) and rotational displacement $R\langle \theta^T \rangle$ trajectories (b). To compute this trajectories we average over particles with comparable mid-cycle displacements represented by different colors. All units in mm. The mid-cycle displacements go from $\mu^C = 6 \times 10^{-2}\, mm$ to $3\, mm$ for translations and from $R\theta^C = 1 \times 10^{-1}\, mm$ to $3\, mm$ for rotations. Results for 2.5% compression amplitude.

per particle. We have verified that varying r_c such that the mean number of contacts per particles is between 4, the isostatic limit for frictional particles [21], and 6, the jamming point, does not change the quantitative results presented here.

We define χ_i^T as the total number of contacts of an individual particle at time T. While the translational displacement are weakly correlated with the number of contacts a particle have at the beginning of the cycle, the rotational displacement are strongly dependent on this quantity as shown on Figure 10. Particles with fever contacts tend to have much bigger end of cycle rotations. This suggests that particles that can rotate more freely, are less prone to return to their original positions. Note that in frictional contacts the transition between the "rolling" and "slipping" phases is hysteretical. This means than even a conservancy of contact points does not guarantee the reversal of rotational motion. Indeed, while we find that both translational and rotational irreversibility are strongly correlated with a gain or loss of a

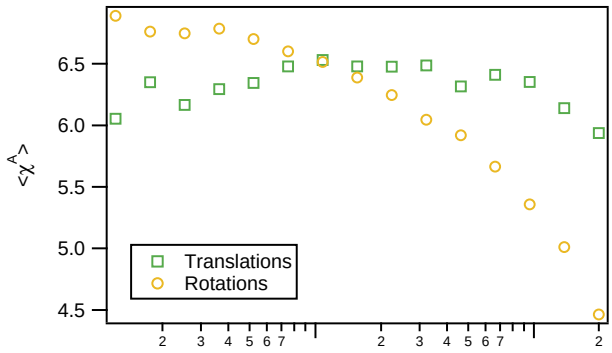

Figure 10. The mean number of contacts at the beginning of cycle as a function of translational and rotational displacements. Displacements in mm. Results for 2.5% compression amplitude.

contact (not shown), translations are more affected.

VI. SUMMARY AND CONCLUSIONS

We conducted a novel experiment allowing us to track translations and rotations of particles in three dimensions during cycles of uni-axial compression. We found that the overall reversibility of translations is much higher than that of rotations. This is explained by the absence of direct correlations between the rotations and translations; the reversible motion of particles "trapped" in cages [16] does not imply the reversibility of rotations. Given the available results of a presence of correlations between translations and rotations for ellipsoid particles [12], a larger correlation between translations and rotations may be observed for larger friction and different frictional properties of the particles. In our system, the non-reversibility of rotations is a possible mechanism for the system to maintain a memory of cycling, even under small forcing conditions that do not imprint a memory in "bulk" indicators of prior forcing (segregation, compaction).

Even though most particles retain their neighbors in our experiment, their contact-point dynamics follows a more hysteretic path and rotational motion is not reversible. It is highly probable that the irreversibility of rotations is also reflected in a parameter which we cannot track in our experiments: the force distributions. To elucidate this hypothesis, further work is needed to track the rotations and the forces on the particles at the same time, either through simulations or different experimental methods [22]. Another important aspect of granular flow is the vector of rotation compared to the direction of shear/compression. It has been predicted [23] that particles will rotate perpendicular to the shearing motion. However, to verify this hypothesis experimentally, we need to access all three degrees of rotations, which will be the subject of our future work.

Note that measurements of rotations are particularly valuable in dense systems such as ours, where translational motion is suppressed and the main mechanism of energy dissipation is by friction between the particles. Frictional dissipation manifests itself in rotational motion, not translation, and thus particle rotations are the key to gain insights into the energetics of dense granular flow. We expect that the experimental data presented here will allow for more direct validation of the competing approaches toward simulating frictional dissipation [24, 25].

We are grateful to Zackery Benson, Jacob Prinz, Charlotte Slaughter and Dara Storer for their help with the experiments. This work was supported by National Science Foundation grant DMR5244620. C. S. and D. S. were supported by TREND, an NSF REU program PHY1756179.

[1] M. Hecke, Journal of Physics: Condensed Matter **22**, 033101 (2010).
[2] F. Rietz, C. Radin, H. Swinney, and M. Schröter, Physical Review Letters **120**, 055701 (2018).
[3] A. Panaitescu, K. Reddy, and A. Kudrolli, Physical Review Letters **108**, 108001 (2012).
[4] A. Tordesillas, D. Walker, and Q. Lin, Physical Review E **81**, 011302 (2010).
[5] L. Srinivasa Mohan, K. Kesava Rao, and R. Nott Prabhu, Journal of Fluid Mechanics **457**, 377 (2002).
[6] A. Kasahara and H. Nakanishi, Physical Review E **70**, 051309 (2004).
[7] T. Matsushima, H. Saomoto, Y. Tsubokawa, and Y. Yamada, Soils and Foundations **43**, 95 (2003).
[8] J. Zhang, R. Behringer, and I. Goldhirsch, Progress of Theoretical Physics Supplement **184**, 16 (2010).
[9] J. Wenzl, R. Seto, M. Roth, H.-J. Butt, and G. Auernhammer, Granular Matter **15**, 391 (2013).
[10] F. Guillard, B. Marks, and I. Einav, Scientific Reports **7**, 8155 (2017).
[11] B. Kou, Y. Cao, J. Li, C. Xia, Z. Li, H. Dong, A. Zhang, J. Zhang, W. Kob, and Y. Wang, Nature **551**, 360 (2017).
[12] B. Kou, Y. Cao, J. Li, C. Xia, Z. Li, H. Dong, A. Zhang, J. Zhang, W. Kob, and Y. Wang, Physical Review Letters **121**, 018002 (2018).
[13] S. Hall, M. Bornert, J. Desrues, Y. Pannier, N. Lenoir, G. Viggiani, and P. Besuelle, Geotechnique **60**, 315 (2010), `http://dx.doi.org/10.1680/geot.2010.60.5.315`.
[14] M. Harrington, M. Lin, K. Nordstrom, and W. Losert, Granular Matter **16**, 185 (2014).
[15] M. Harrington, J. Weijs, and W. Losert, Physical Review Letters **111**, 078001 (2013).
[16] J. Royer and P. Chaikin, Procedeengs of National Academy of Science **112**, 49 LP (2015).
[17] J. Dijksman, F. Rietz, K. Lőrincz, M. van Hecke, and W. Losert, Review of Scientific Instruments **83**, 011301 (2012).
[18] T. Marschall, Y.-E. Keta, P. Olsson, and S. Teitel, Phys-

ical Review Letters **122**, 188002 (2019).
[19] M. Bandi, H. E. Hentschel, I. Procaccia, S. Roy, and J. Zylberg, EPL (Europhysics Letters) **122**, 38003 (2018).
[20] A. Peshkov et al., under preparation.
[21] M. Hanifpour, N. Francois, V. Robins, A. Kingston, S. Vaez Allaei, and M. Saadatfar, Physical Review E **91**, 062202 (2015).
[22] R. Hurley, S. Hall, J. Andrade, and J. Wright, Physical Review Letters **117**, 098005 (2016).
[23] T. Halsey, Physical Review E **80**, 011303 (2009).
[24] K. Bagi and M. Kuhn, Journal of Applied Mechanics **71**, 493 (2004), 10.1115/1.1755693.
[25] Y. Wang, F. Alonso-Marroquin, and W. Guo, Particuology **23**, 49 (2015).